PAPER

Solvent-dependent on/off valving using selectively permeable barriers in paper microfluidics†

G. IJ. Salentijn,[ab] N. N. Hamidon[a] and E. Verpoorte[*a]

We report on a new way to control solvent flows in paper microfluidic devices, based on the local patterning of paper with alkyl ketene dimer (AKD) to form barriers with selective permeability for different solvents. Production of the devices is a two-step process. In the first step, AKD-treated paper (hydrophobic) is exposed to oxygen plasma for re-hydrophilization. 3D-printed masks are employed to shield certain areas of this paper to preserve well-defined hydrophobic patterns. In the second step, concentrated AKD in hexane is selectively deposited onto already hydrophobic regions of the paper to locally increase the degree of hydrophobicity. Hydrophilic areas formed in the previous oxygen plasma step are protected from AKD by wetting them with water first to prevent the AKD hexane solution from entering them (hydrophilic exclusion). Characterization of the patterns after both steps shows that reproducible patterns are obtained with linear dependence on the dimensions of the 3D-printed masks. This two-step methodology leads to differential hydrophobicity on the paper: (i) hydrophilic regions, (ii) low-load AKD gates, and (iii) high-load AKD walls. The gates are impermeable to water, yet can be penetrated by most alcohol/water mixtures; the walls cannot. This concept for solvent-dependent on/off valving is demonstrated in two applications. In the first example, a device was developed for multi-step chemical reactions. Different compounds can be spotted separately (closed gates). Upon elution with an alcohol/water mixture, the gates become permeable and the contents are combined. In the second example, volume-defined sampling is introduced. Aqueous sample is allowed to wick into a device and fill a sample chamber. The contents of this sample chamber are eluted perpendicularly with an alcohol/water mixture through a selectively permeable gate. This system was tested with dye solution, and a linear dependence of magnitude of the signal on the sample chamber size was obtained.

Introduction

In recent years, there has been an increasing interest in cheap analytical devices for a number of reasons.[1–5] First of all, point-of-care diagnostics are becoming more important; both scientists and medical professionals are recognizing the value of being able to diagnose and monitor patients *outside* the

a Pharmaceutical Analysis, Groningen Research Institute of Pharmacy, University of Groningen, Antonius Deusinglaan 1, P.O. Box 196, 9700 AD Groningen, The Netherlands. E-mail: E.M.J.Verpoorte@rug.nl; Fax: 050 363 75 82; Tel: 050 363 33 37
b TI-COAST, Science Park 904, 1098 XH Amsterdam, The Netherlands

† Electronic supplementary information (ESI) available: 3D printer settings; additional characterization of paper microfluidic structures: (1) 75% methanol in water instead of water, (2) influence of varying oxygen plasma exposure, (3) different concentration of AKD for the initial patterning; visualization of the porous cellulose network in untreated and AKD-patterned paper; demonstration of sample sink and optimized perpendicular elution in the volume-defining sampling device; concentration dependence of the signal obtained with yellow dye solution; evidence for an evaporation effect during sampling to justify normalization; effect of normalization on volume-defined sampling results. See DOI: 10.1039/c5lc01355k

clinical environment.[1,2] Improved therapeutic drug monitoring and more intensive observation of physiological values to optimize therapy are as important as providing more comfort for patients, who can perform the tests themselves at home or at a physician's office. Second, there is a growing awareness that robust, yet cheap and mobile, diagnostic tools are very much needed in low resource settings, where levels of public health are dramatically lower than in the western world.[3,4] In environmental and forensic science too, analysis and interpretation of results are mostly restricted to stationary laboratories. Providing tools to perform analysis on the spot could greatly benefit the efficiency and accelerate the outcomes of such analyses.[5]

Great effort is being spent to realize these ambitious goals in a number of fields. The use of paper has recently re-emerged in the field of microfluidics,[6–9] after its first introduction in the late forties.[10] The creation of hydrophobic patterns on paper, with *e.g.* wax,[6] alkyl ketene dimer (AKD),[7] polydimethylsiloxane (PDMS)[8] or photolithography,[9] allows fluid movement within the resulting confined hydrophilic regions (*i.e.* the regions which have not been treated). This

hydrophobic patterning enables channel fabrication, directional control over fluid flows and thus the production of cheap and disposable analytical devices. However, simply confining liquids to specifically designed channels and subsequently leading them to reaction chambers with pre-deposited reagents is merely the first step. In order to perform more challenging analyses on a paper-based platform, tools for fluid manipulation are required. There have been numerous reports of ways to control solvent flows, such as mechanical valving by connecting or disconnecting the hydrophilic pathway manually,[7,11] the integration of dissolvable barriers or fluidic timers for controlled solvent delivery/reagent release,[12] and the combination of paper and plastic to manipulate fluid flow velocity.[13] However, thus far there are no reports of permanent barriers for reusable on/off valving to control flows within paper devices.[14] In this work, we introduce the concept of selective permeability of hydrophobic barriers, based on AKD patterning. These barriers act as on/off valves to stop or allow the movement of solutes through a paper device, depending on the choice of solvent. Patterning with different concentrations or loads of AKD in hexane allows the fabrication of hydrophobic barriers with differential permeability. Barriers formed with a low AKD load can confine aqueous solutions; however, alcohol or alcohol/water mixtures easily enter the AKD domain. By using a second, high-load AKD patterning step, we can confine some of the solvents (mainly alcohol/water mixtures) that can leak through low-load AKD barriers. When the high-load AKD is used to make channel walls and the low-load AKD for so-called 'gates', one has introduced valves into the device that can be switched on and off by changing the solvent.

For the first low-load patterning step, a method for hydrophobic patterning of paper with 3D-printed masks is used, based on the AKD bonding/plasma treatment method published by Li et al.[7] It has been recognized that AKD patterns can confine some solutions/solvents, while other solvents, such as alcohols, tend to leak through these patterns.[15] In order to also confine water/alcohol mixtures, we reapply AKD solution at a higher concentration (high-load AKD) onto the already hydrophobic structure produced in the initial step. Prior to this application, the hydrophilic regions are wetted with water, which excludes the hexane solution of AKD from entering them, due to the immiscibility of both solvents (hydrophilic exclusion). A thorough characterization of the quality of paper microfluidic devices produced with our method is presented.

The selective permeability of these gates can be used to load chambers with aqueous solutions of reagents/samples, which, after drying, can be mixed by elution with an alcohol/water mixture into a single chamber. Selective permeability can also be employed for quantitative sampling of water sources for perpendicular processing/detection. A proof-of-concept is given for both of these applications.

Materials and methods

Chemicals and disposables

A strip (20 mm wide) of grade-1 chromatography paper (Whatman, Maidstone, England) was used as the paper substrate. AKD, a sizing agent used in the paper-making industry, was kindly given to us by Ashland Inc. (Tampere, Finland). Analytical-grade hexane (Biosolve B.V., Valkenswaard, The Netherlands) was used for the dissolution of AKD (0.6 g L^{-1} for low-load application and 5.0 g L^{-1} for high-load application). The application of the hexane solutions of AKD onto paper was carried out in a fumehood. Millipore water and absolute methanol (Biosolve B.V., Valkenswaard, The Netherlands) were used for the characterization of the AKD patterning. Millipore water and 96% ethanol (VWR International B.V., Amsterdam, The Netherlands) were used to test the selectively permeable on/off valving devices. Arnitel Eco (d = 1.75 mm, DSM, Geleen, The Netherlands) and polylactic acid (PLA, EasyFil d = 1.75 mm, Formfutura, Amsterdam, The Netherlands) filament were used for the production of mask parts by 3D printing for the AKD-patterning protocol. Acrylonitrile butadiene styrene (ABS, d = 1.75 mm, Kunststofshop, Zevenaar, The Netherlands) filament was used for the production of a clamping system. Blue (mix of E133 and E122), red (E122) and yellow (mix of E102 and E124) food dyes were purchased at a local grocery store and diluted in water to be used as model compounds in the demonstration of selective permeability.

Design and fabrication of 3D-printed parts

The design of parts for 3D printing, as well as the 3D-printing process is described in detail in previous work.[13] In summary, designs were made with a 3D-drawing program (Solidworks, Waltham, MA, USA), loaded into the operating program (RepetierHost) for the 3D printer (Felix, de Meern, The Netherlands, version 3.0). The model was translated by slicing software (SFact, Skeinforge) into a G-code (a coordinates file) on which the printer could operate. Polymer filament was extruded through a heated nozzle (diameter = 0.35 mm) and deposited on a heated bed to build the structures. For this work, the printer was upgraded to v3.0, with parts of higher quality as compared to the v1.5. Masks for the AKD patterning were partially printed in PLA and partially in Arnitel. During production, the print job was paused after printing 12 layers in PLA. The filament was then exchanged, and the print job was resumed with Arnitel at 60% of the print speed, in order to properly print this material.

Clamp parts were printed in ABS, which is prone to warping (i.e. shrinkage in a part due to differences in internal temperature). In order to properly print ABS parts, a layer of PLA was printed and then taped to the heated bed first; afterwards the ABS was printed on top of the PLA. Table S1 in the ESI† provides settings in the slice and print software for the above-mentioned parts for the Felix v3.0.

AKD patterning: step 1 (low AKD load)

This work adapted the method published by Li *et al.*[7] for making paper microfluidic devices by AKD treatment and subsequent exposure of selected areas to oxygen plasma for re-hydrophilization. Instead of the metal masks used by Li *et al.*,[7] we used 3D-printed masks to shield certain regions of the paper to preserve hydrophobicity (Fig. 1). First, cellulose paper was briefly dipped into a 0.6 g L^{-1} hexane solution of AKD and dried. The paper was then put into an oven for 30 min at 100 °C to melt and spread the AKD, and covalently bond it to the hydroxyl residues on the cellulose, which made the paper hydrophobic.[16] 3D-printed mask parts were designed to shield certain regions of the paper from oxygen plasma (which re-hydrophilized the AKD-treated paper) while leaving other areas exposed. Exposed areas thus became the hydrophilic channel and chamber structures, whereas the shielded regions became the hydrophobic barriers.

The mask parts were partially printed in PLA. Half-way during the print, the material was changed to Arnitel, which retained its elasticity after the printing process (Fig. 1A). The part of the mask meant to contact and thus shield the paper was printed in the flexible Arnitel material, to provide a tighter seal against the plasma upon application of pressure onto the masks. Two masks (mirror images) were needed: one for each side of the paper (Fig. 1B). Continuous ridges (1 mm height by design) were incorporated around the periphery of the mask and around all openings in the mask. In this way, the masks sealed b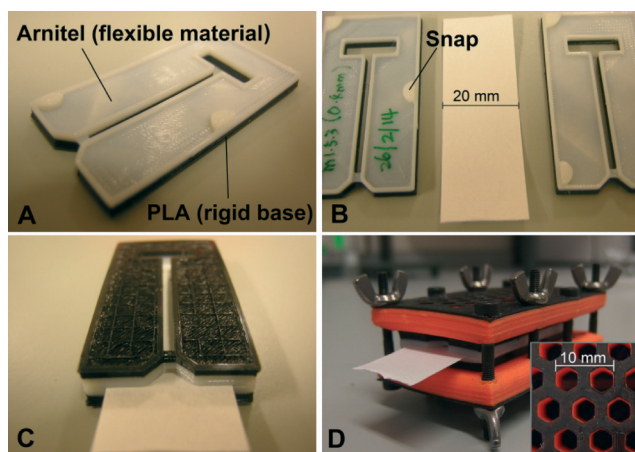etter to paper regions that needed to remain hydrophobic upon application of pressure onto the mask. Furthermore, the masks contained snap connections for alignment and fixation of the two mask parts (Fig. 1B). On the PLA side, identical ridges to those on the Arnitel side were fabricated (Fig. 1C) in order to provide pressure only where it was most needed (*i.e.* at the borders between hydrophobic and hydrophilic regions). The relative rigidity of PLA provided a better distribution of pressure onto the masks than would have been the case if the entire mask had been printed in Arnitel.

Next, a clamping system, with honeycomb cavities (Fig. 1D, inset) to allow the free flow of gas/plasma through the clamp to open mask regions, was 3D printed in ABS. This clamp could be tightened with screws and was used to apply pressure to the masks and seal off the selected areas of the paper (Fig. 1D). This assembly was put into the plasma cleaner (PDC-0002, Harrick Plasma, Ithaca, NY, USA) and exposed to oxygen plasma for 30 seconds. The oxygen plasma was generated at a pressure between 450–460 mTorr and the power used was 29.6 W.

AKD patterning: step 2 (high AKD load)

A second application of AKD was implemented in the fabrication process in order to increase the hydrophobicity in the
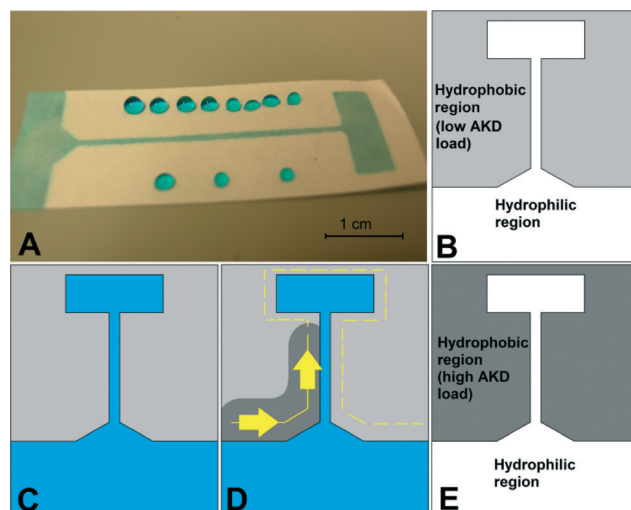

Fig. 1 3D-printed tools for the fabrication of AKD patterned paper microfluidic devices. (A) A mask part made of PLA (lower half, black) and flexible Arnitel (upper half, white). The rigid PLA base allows equal distribution of pressure over the mask, whereas the Arnitel top allows a tight seal upon the application of pressure. (B) Two mirror-image mask parts, which can be aligned with snap connections and an AKD-coated piece of chromatography paper. (C) The paper is sandwiched between the mask parts. The rigid PLA base, as well as the Arnitel top, contain ridges to focus pressure on the borders between shielded and non-shielded areas of the paper. (D) The mask and paper sandwich is put into an ABS clamp containing honeycomb cavities (inset) and pressure is applied by tightening the screws. The assembly is then exposed to oxygen plasma to re-hydrophilize the unshielded areas.

Fig. 2 Second application of AKD (5.0 g L^{-1}) to increase hydrophobicity. (A) Paper device after the first low-load AKD application step. An aqueous blue dye solution was applied to both the hydrophilic and hydrophobic domains to demonstrate wettability by water. The hydrophilic domains were wetted, whereas the solution formed droplets on top of the hydrophobic areas. (B) Schematic design of the device in A. (C) The hydrophilic area was wetted with water for the second AKD application. (D) A 5.0 g L^{-1} hexane solution of AKD (high-load) was applied *via* a syringe on a pump to the hydrophobic domain, by manually moving a flexible capillary tip along the borders between the hydrophilic and hydrophobic regions. As the hydrophilic regions were filled with water, the hexane containing AKD did not enter into those regions (hydrophilic exclusion). Afterwards, the paper was put into the oven at 80 °C for 3 min. (E) The hydrophobic regions became more hydrophobic, whereas the hydrophilic regions remained unchanged.

patterns (Fig. 2). A hexane solution of 5.0 g L^{-1} AKD was prepared and approximately 100 μL was loaded into a 100 μL gastight syringe (#1710, Hamilton, Reno, NV, USA). The syringe tip was connected to a fused silica capillary (ID = 0.25 mm, Polymicro Technologies, Phoenix, AZ, USA) *via* a small length of Tygon tubing (ID = 0.25 mm, Gilson, Middleton, USA). The syringe was fit onto a syringe pump (ProSense B.V., Oosterhout, The Netherlands) and the hydrophilic structures in the paper device were wetted with water (Fig. 2C). The content of the syringe was applied to the hydrophobic regions of the paper device by manually moving the end of the capillary along the wetted borders of the hydrophilic areas (Fig. 2D) at a flow rate of 30 μL min^{-1}. Due to the immiscibility of water and hexane, the AKD solution did not enter the hydrophilic domains (hydrophilic exclusion), resulting in no modification of those hydrophilic areas, while the hydrophobic domains became more hydrophobic (Fig. 2E). At least three passages were made along each border, and the application continued until the syringe had been emptied. Due to the fact that the hexane evaporated within a few seconds after application, the paper was dry when the AKD solution was applied for consecutive times. Afterwards, the hydrophilic areas were re-wetted and the wetted paper devices were put into an oven for 3 min at 80 °C.

Characterization of AKD patterning

The design shown in Fig. 1 and 2 was used to characterize the patterns which were obtained after both AKD application steps. Four different sets of masks with different channel widths were 3D printed (0.5, 1.0, 1.5 and 2.0 mm by design). In all cases, the length of the channel was 35 mm and the dimensions of the box at the end of the channel were 5 mm by 15 mm. Five paper devices were produced with each mask; these were then characterized and subsequently subjected to the second AKD application. The paper devices were examined by wetting the channels with water and taking a photograph (Nikon Coolpix 8400) under the microscope (Leica S8APO, Leica Microsystems, Wetzlar, Germany). A ruler was used in each photograph for size calibration (Fig. 3A). The wetted channel was measured using the image analysis software ImageJ[17] and the absolute width was calculated based on the dimensions of the ruler. The patterns obtained after the second application were also tested with water/methanol 1:3 (v/v) by using the same protocol. The actual channel width of the channel structure in the 3D-printed masks was also measured in this way. All measurements were performed by three researchers, and the values were averaged in order to minimize errors introduced by manually measuring the dimensions. This methodology for the characterization was used for two important reasons: (i) the channel structures are only visible when wetted, and (ii) this approach is pragmatic in the sense that we are specifically interested in the width of the wetted channel, because that is the dimension which matters during an actual experiment.

The hydrophobicity of the paper after both AKD steps was characterized by measuring the contact angle of 10 μL water droplets on a low-load and a high-load AKD surface (n = 3 droplets per surface). This was achieved by taking a photograph of the droplets from the side, after which the contact angle was determined using an ImageJ plugin (http://rsb. info.nih.gov/ij/plugins/contact-angle.html).

Furthermore, the mass ratio of AKD/paper was estimated for both steps, based on the weight and volume of a 2 by 3 cm piece of paper (which is in the size range of the devices demonstrated in this work) and the concentrations of the AKD solutions.

Finally, patterned paper from both application steps, as well as untreated cellulose paper, were visually inspected under an inverted microscope (Leica DMIL mounted with a DFC365 FX camera, Leica Microsystems, Wetzlar, Germany) to determine whether physical deposition of AKD into the pores and/or modifications to the porous network could be observed.
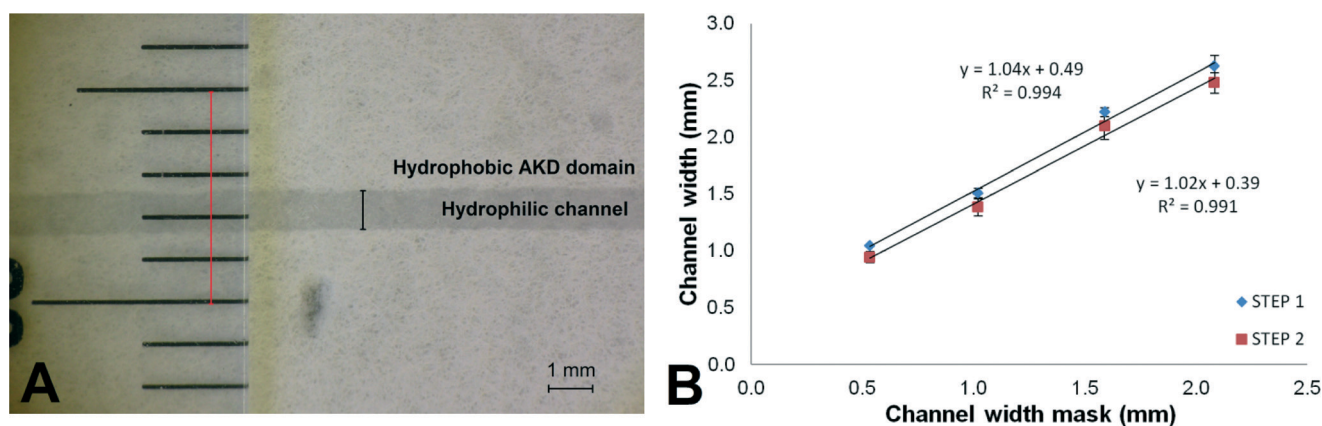

Fig. 3 Characterization of both AKD application steps. (A) The channel width was measured with ImageJ from a photograph in which the channel was wetted with water and a ruler was used as size reference. The actual channel width was calculated by multiplying the ratio between the black vertical bar and the red vertical bar by 5 mm. (B) The average channel width (n = 5 devices per data point) is plotted *versus* the channel width of the 3D-printed mask parts for both application steps. Error bars show the standard deviation.

Design and fabrication of devices to demonstrate selective permeability

Designs for paper microfluidic structures were made based on the concept of selective permeability. In these devices, three distinct features could be distinguished: (i) hydrophilic regions, (ii) low-load AKD gates and (iii) high-load AKD walls. The gates were located between hydrophilic regions and were not included in the second AKD application. Due to the fact that these gate structures were thin (generally 1 mm) and surrounded by wetted hydrophilic regions during the second application, the AKD would not travel into these regions, thus they retained their original (lower) hydrophobicity.

Two different devices were designed and fabricated to demonstrate the potential of selective permeability. The first device was designed to conduct multi-step chemical reactions, and contained adjacent chambers, separated by low-load AKD gates. These chambers could be loaded with aqueous sample or aqueous reagent solutions without any interaction between the different solutions. The content of the chambers could then be mixed upon elution with a solution of ethanol/water 1:1 (v/v). The second device was designed for volume-defined sampling of a liquid. It contained a channel for loading liquid sample to fill a sample chamber and an adjacent sample sink. The content of the sample chamber could then be eluted perpendicularly for downstream processing and/or detection. Elution of the sample into a collection chamber was performed with a mixture of ethanol/water 55:45 (v/v). Different volumes of the sample chamber were tested to assess whether a correlation could be found between volume of the chamber and (i) the amount of sample which was loaded into the device and (ii) the amount of sample that was eluted. In both devices, aqueous dye solutions were used to demonstrate the feasibility of the designs.

Image analysis

Images were taken and analyzed in order to quantify the amount of dye that was sampled with the volume-defined sampling devices. A scan (600 dpi, full colour) of the paper device (after loading with sample, as well as after elution) was opened in *hue*, *saturation*, *brightness* (HSB) display and the saturation values were used for dye quantification. The area of interest (either the sample chamber or the collection chamber) was selected, and the total saturation of that area was used as a measure for the amount of dye present in that area. Values were normalized to compensate (i) for differences between scans (by using a reference spot) and (ii) for evaporation-based concentration differences (by using the average saturation in the sample supply channel).

Results and discussion

Characterization of AKD patterning

Fig. 3 shows the results of the characterization of both AKD application steps. The averages of the measured channel widths on paper (n = 5 devices per channel width) are plotted against the measured widths of the channel structure in the 3D-printed masks (Fig. 3B). Error bars show the standard deviation. The channel widths shown in Fig. 3B are measured in water-filled devices. The hydrophobic structures made with the first AKD step alone can confine water (contact angle of 94.9°; standard deviation (sd) = 2.9°), yet are permeable to most mixtures of water with alcohols. Structures which undergo both AKD application steps can contain water (contact angle of 116.5°; sd = 2.0°) and up to 75% methanol in water (ESI,† Fig. S1), and 55% ethanol in water (see next section). There is no apparent difference in channel width when 75% methanol in water is used to wet the channels instead of just water. The mass ratio of AKD/paper for step 1 (approximately 0.1%) and step 2 (approximately 1%) are fairly low. No higher amounts are required, as the mechanism of fluid confinement revolves around altering the surface energy of the cellulose fibers, rather than physically blocking the pores. Patterning of paper with AKD in these quantities also appears to have little effect on the pore size and the porous cellulose network, based on microscopic observation (ESI,† Fig. S2). Obviously, the hydrophobicity cannot be increased beyond the hydrophobicity of AKD itself. Fig. 3 demonstrates that it is possible to fabricate paper microfluidic structures of reproducible size, and with linear dependence on the dimensions of the 3D-printed mask parts. Exposure of unshielded areas to oxygen plasma leads to broadening of this area in relation to the dimension of the corresponding structure in the 3D-printed masks, by an amount equivalent to the *y*-intercept. This broadening can be explained by the fact that the oxygen plasma can penetrate the paper and travel through it.[7]

Although the authors of the original method did not report a characterization of their fabrication process and the resulting devices, what information is given seems to be in line with our work. In the original study, the channel width, due to oxygen plasma exposure, increased by approximately 0.3 mm in comparison to the original mask width (1 mm) after 15 s of plasma exposure (15 W).[7] In our study, the channel width increased by approximately 0.5 mm (for the first application step). However, we used an oxygen plasma exposure of 30 s (29.6 W), which is substantially greater than the exposure in the original study. Longer exposure times to oxygen plasma lead to broader hydrophilic structures (ESI,† Fig. S3 and S4). However, our experiments showed that a shorter or weaker exposure can lead to incomplete hydrophilization of the exposed regions.

The hydrophobicity of the AKD patterns was increased in order to broaden the range of solvents which can be confined within a channel or chamber. There were two main reasons for the introduction of the second AKD application step, instead of simply treating the entire paper with a higher concentration of AKD at the beginning. The first reason is related to the above-mentioned broadening of channel structures during extended plasma treatment. The use of a higher AKD concentration on the entire paper would require extended plasma treatment to regain hydrophilicity in the unshielded regions, and thus result in increased channel width (ESI,† Fig. S4 and

S5). Secondly, it is unknown whether and what kinds of residues remain in the hydrophilic domain after the plasma treatment. An increase in the AKD load in the first patterning step would result in an increase of such residues in the hydrophilic regions as well. The second application step ensures that, due to hydrophilic exclusion, the highly concentrated hexane solution of AKD cannot enter the hydrophilic regions. Fig. 3B shows that, after the second application, the channel width was smaller than after the first step. We suspect that this narrowing was caused by the final oven step, in which the AKD melts and possibly spreads into the hydrophilic regions to some extent.

There are both advantages and drawbacks to this method for making paper microfluidic devices. First, there is the advantage of 3D-printed masks over masks produced by other methods, as 3D printing allows for easy rapid prototyping on an inexpensive instrument. Secondly, 3D printing allows the use of flexible material for the layer in contact with the paper for a tighter seal. Finally, the combination of two application steps allows the use of different concentrations of AKD in a single paper device, as demonstrated in the next sections. The second AKD application can be combined with other initial patterning strategies, such as the original AKD method with metal masks,[7] the method in which the sizing agent is applied via an inkjet printer,[18] or even unrelated fabrication techniques for paper microfluidic devices. Moreover, the hydrophobic agent in the second application step might also be varied, as long as it can be dissolved in a solvent that is immiscible with water. This could lead to wall structures with greater hydrophobicity, which would increase the range of solvents that can be used in devices with on/off valving based on selective permeability. On the other hand, this method is time-consuming, and more rapid techniques would be necessary for mass production.

Selective permeability – separate, connectable chambers

Fig. 4 presents the first demonstration of on/off valving using selective permeability. The device shown contains three hydrophilic chambers and a hydrophilic entry region, connected by low-load AKD valves. Surrounding these hydrophilic areas is a high-load AKD wall (Fig. 4A). The hydrophilic chambers can confine water (Fig. 4B) or aqueous solutions

(of dyes in this case, Fig. 4C). After drying (Fig. 4D), samples can be eluted via the entry region and the separately stored dyes are combined (Fig. 4E–G). After the device is dried (Fig. 4H) and again wetted with water (Fig. 4I), the valves are still intact. This design can be employed for separately spotting different aqueous solutions of reagents in the chambers for multi-step chemical reactions. Separately loading reagents is important (i) in reactions where the reagents might react without the presence of analyte, (ii) when there is competition between the reagents for the analyte, and (iii) when the order in which the reagents react matters (e.g. the colorimetric reaction of nitrite with Griess reagents).[19]

One important feature of the low-load AKD valves is that their permeability is determined not only by the AKD concentration and the choice of solvent, but also by their position in the device. Capillary action is determined by the length of the fluid front, and fluid progression decreases with an increase in this length.[20] In the case of selective permeability, the same rules apply: the further a gate is located from the eluent source, the more difficulty the eluent will have to overcome the barrier. This effect can be seen with the gate between the top two chambers in the device in Fig. 4G, where a part of the gate is not completely permeable. This property should be taken into account when designing devices with selectively permeable valves. One way to compensate for this effect could be to design valves with narrower dimensions.

Selective permeability – volume defined sampling

Fig. 5 shows another application of selective permeability. The device (Fig. 5A) was designed for sampling a defined volume of liquid from e.g. natural water sources. Sample solution wicks into the device once it is dipped into the source (from left to right). It enters a chamber through a supply channel and then continues to wick into a circular sample sink. The sample sink was introduced into the design to prevent a sampling bias. Due to retention of solutes on the paper, the fluid front usually consists of mainly water. Integrating a sample sink ensures that this diluted fluid front is not included in the sampling process (ESI,† Fig. S6). After the sample has dried, it can be eluted perpendicularly with 55% ethanol in water. The design of the device was optimized to include only the content
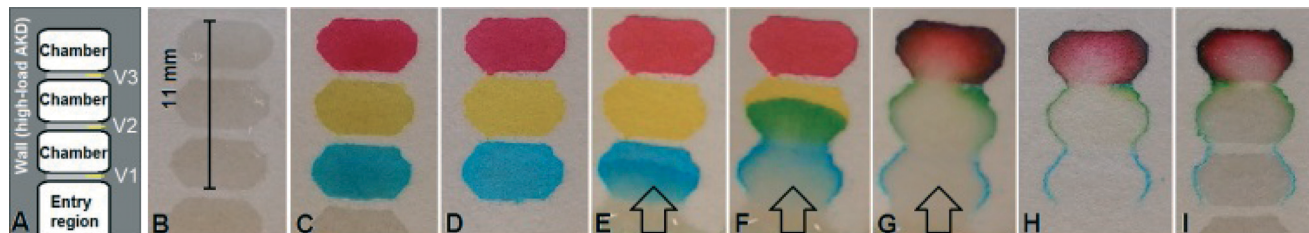

Fig. 4 Paper microfluidic device based on selective permeability for multi-step chemical reactions. (A) Schematic overview of the device, which contains hydrophilic regions (white) separated by low-load AKD valves (light gray, V1–V3), the total of which is surrounded by high-load AKD walls (dark gray). (B) An actual device in which the hydrophilic regions are wetted with water. (C) The three chambers are filled with aqueous solutions of different dyes (4 μL) and (D) dried. (E–G) The device is dipped into 50% ethanol in water for elution of the dyes through the selectively permeable valves. Upon elution, the different dyes mix and end up in the top chamber. (H) The device is dried and (I) rewetted with water to demonstrate that the valves are still intact.
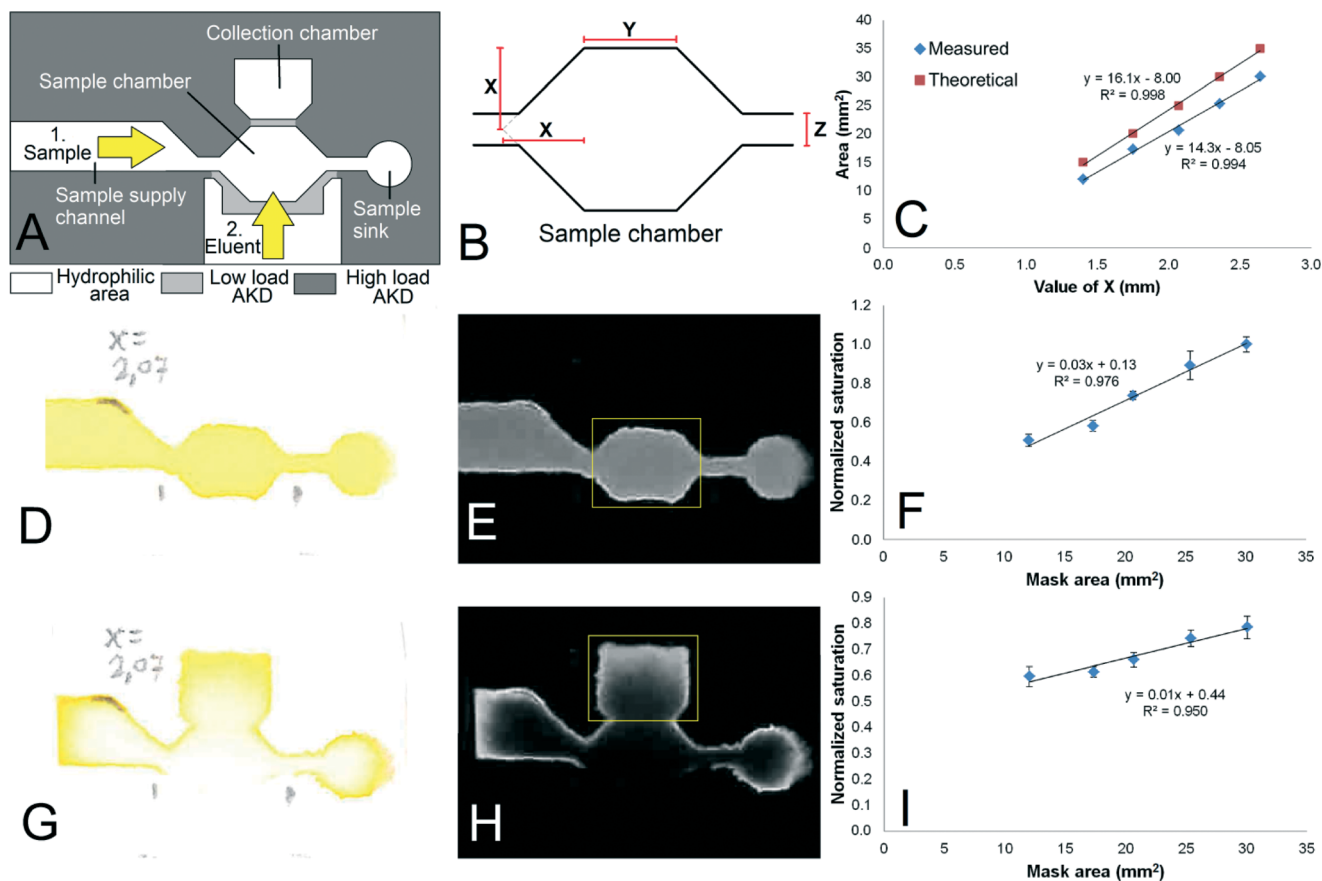
Fig. 5 Volume-defined sampling with a paper microfluidic device. (A) Schematic representation of the device. White areas are hydrophilic, light gray areas have a low AKD load (valves) and dark gray areas have a high AKD load (walls). Sample can be loaded into this device *via* the left supply channel (labeled '1. Sample'). Sample wicks into a sample chamber and later into a sample sink, designed to prevent sampling bias. After the sample has dried, it can be eluted perpendicularly with 55% ethanol in water *via* the bottom entry channel (labeled '2. Eluent'). Due to the design, sample from within the sample chamber will be eluted upwards and collected in the upper collection chamber. Sample in other parts of the device will be drained *via* the sample supply channel or into the sample sink. (B) Schematic overview of the sample chamber. The value of X is varied in order to produce devices with different volumes for the sample chamber. The respective values for Y and Z are 4 mm and 0.5 mm. (C) Relation between the actual and theoretical areas of the sample chamber in the 3D-printed mask and the value of X. (D) Example of a device loaded with yellow dye solution. (E) The same device in HSB display (saturation) in ImageJ, which is used to quantify color in a certain region of the device. The total saturation of the area within the yellow lines was quantified. (F) The normalized saturation of the sample chamber is plotted against the area of the sample chamber in the mask (n = 3 devices per mask). Error bars show the standard deviation. (G–I) Same as D–F, but after elution and measured in the sample collection chamber. This last series represents the sample that can be used for downstream processing and/or detection.

of the sample chamber in the sampling process upon elution, while the contents of the supply channel and the sample sink are removed *via* those respective routes (ESI,† Fig. S7). In these experiments, dyes were used as model compounds to demonstrate the concept of selective permeability, and how it can be applied to user-friendly, volume-defined sampling. For any real application, the collection chamber might contain a reagent for a colorimetric test, or lead to a detection system such as a mass spectrometer.[21] Depending on the actual application, the dimensions of the device might need to be adapted. The key factor in this is the retention of the analyte of interest on paper. Compounds with a strong retention will require a relatively large sample sink, as well as a larger collection chamber to ensure the definition of an unbiased sample and complete sample collection, respectively.

In order to demonstrate the volume-defining aspect of this device, five different masks with different sizes for the sample

chamber were designed and produced. Fig. 5B shows the schematic for this part of the device. The value of 'X' in this scheme was varied (X = 1.40, 1.75, 2.07, 2.36 or 2.64) to create these different sizes. After production of the masks, the area of the sample chamber in the masks was measured with ImageJ and plotted against the value of 'X' used in that design. The theoretical areas of the sample chambers (according to the Solidworks drawing) are included in this graph (Fig. 5C). This result shows that there is a minor discrepancy between the sizes of the sample chamber in the design and in the actual mask parts, which is a recurring problem with hot-extrusion based 3D printers. For this reason, the actual mask size was used in the data analysis.

Dependence of saturation on concentration

Yellow dye solution was used as a model to test the quantitative sampling capabilities of this system. The HSB color space

was used for image analysis. This color space has been used by others in image analysis/quantification,[22,23] but in different ways than it was used here. For this reason, we first verified that a linear relation exists between the concentration of the dye and the saturation which is measured (ESI,† Fig. S8). Next, paper devices were produced using the 5 different sets of masks (*n* = 3 per set). A small volume (less than one mL) of sample solution was poured onto a watch glass and used for all fifteen devices. The paper devices were dipped into the yellow dye solution, dried, and scanned from both sides (Fig. 5D). The average saturation in the center of the supply channel was measured (area of approximately 3 × 3 mm, average from both sides), which was used for two purposes: (i) to check whether the values of the saturation were located in the linear range of the detection methodology, and (ii) to check for changes in the concentration of the sample solution over time, due to evaporation. The values for average saturation in the supply channel were thus plotted against the order in which the samples were taken (ESI,† Fig. S9). The results indicate (i) that the values indeed lie within the linear range, and (ii) that the average saturation increases with each subsequent sample, which implies an evaporation effect (*i.e.* the concentration of sample increases due to the evaporation of solvent). For this reason, the average saturation in the supply channel after the sample loading step was used to normalize the values found in the actual image analysis.

Quantification of sample before and after elution

The next step was the analysis of the contents of the sample chamber. The area of interest (the sample chamber in this case) was selected in HSB display (Fig. 5E) and the total saturation in that area (yellow box) was measured and normalized. The normalized total saturation is plotted against the area of the sample chamber in the 3D-printed mask (Fig. 5F). The values for the normalized saturation are given as relative numbers, where the normalized saturation for the largest sample chamber has been given the value of '1'. Error bars show the standard deviation. As can be seen from the results, there is a linear relationship between the area and the normalized total saturation.

The devices were then eluted perpendicularly with 55% ethanol in water (Fig. 5G), and the data acquisition and analysis procedures were repeated, but now for the total saturation in the collection area (Fig. 5H, yellow box). The normalized results of this analysis can be seen in Fig. 5I. Again, the values are related to the normalized total saturation of the largest sample chamber after loading. Error bars show the standard deviation. Again the area of the sample chamber in the masks is directly proportional to the normalized amount of dye that ended up in the collection chamber. This result underlines the added value of systems based on selective permeability, because this device allows for volume-defined sampling that only requires a simple dipping protocol.

The evaporation effect, which was evidently occurring, can (only) be measured and thus corrected for if the analyte itself gives a signal before its elution into the collection chamber (*e.g.* color). If this effect is not corrected for, the variation in the results is much greater, especially after elution (ESI,† Fig. S10). Most applications of this device would be colorimetric reactions, thus normalization is not possible, as the compounds of interest do not give any signal before they are eluted into the collection chamber where they can undergo colorimetric reaction. However, in such cases it is likely that only a single sample will be taken and that the volume of the sample source will be quite large (*e.g.* a lake or a well). As such, evaporation will not have any impact on the outcomes of the test. Nonetheless, this test demonstrates once more how easily measurements from a small sample volume can be negatively influenced by evaporation, and that strict procedures are required for proper quantification.

Conclusions

In this work a new strategy is proposed for the fabrication of paper microfluidic devices. This enables the integration of selectively permeable on/off valves. Selective permeability creates new venues that can be explored in order to design more sophisticated cheap analytical tools, without endangering the user-friendliness.

Two examples of paper microfluidic tools based on selective permeability have been presented, which can easily be implemented in specific designs for well-defined purposes and applications. In conventional microfluidics, integration of valves allows better control over fluid flows and the production of more complex systems. The same goes for paper microfluidics. Up to now, non-mechanical on/off valves have been lacking in the arsenal of paper microfluidics. The introduction of selective permeability can fill this gap.

Future work will focus on expanding the basic concept which has been proposed in this work. More than two concentrations of AKD can potentially be used to allow gradual valving, *i.e.* stepwise modification of the solvent composition would allow progression into new regions of the device with each subsequent step. Furthermore, the choice of the sizing agent can be varied to give differential properties to the cellulose surface. In the same line of thought, hybrid paper microfluidic devices might be very attractive possibilities, which would allow the integration of AKD gates in devices patterned with *e.g.* PDMS or wax.

Acknowledgements

References

1 C. P. Price, *BMJ*, 2001, **322**, 1285–1288.
2 J. Howick, J. W. L. Cals, C. Jones, C. P. Price, A. Plüddemann, C. Heneghan, M. Y. Berger, F. Buntinx, J. Hickner, W. Pace, T. Badrick, A. Van den Bruel, C. Laurence,

H. C. van Weert, E. van Severen, A. Parrella and M. Thompson, *BMJ Open*, 2014, **4**, e005611.

3 C. D. Chin, V. Linder and S. K. Sia, *Lab Chip*, 2007, **7**, 41–57.

4 P. Yager, T. Edwards, E. Fu, K. Helton, K. Nelson, M. R. Tam and B. H. Weigl, *Nature*, 2006, **442**, 412–418.

5 J. G. E. Gardeniers and A. Van den Berg, *Anal. Bioanal. Chem.*, 2004, **378**, 1700–1703.

6 Y. Lu, W. Shi, L. Jiang, J. Qin and B. Lin, *Electrophoresis*, 2009, **30**, 1497–1500.

7 X. Li, J. Tian, T. Nguyen and W. Shen, *Anal. Chem.*, 2008, **80**, 9131–9134.

8 D. A. Bruzewicz, M. Reches and G. M. Whitesides, *Anal. Chem.*, 2008, **80**, 3387–3392.

9 A. W. Martinez, S. T. Phillips, M. J. Butte and G. M. Whitesides, *Angew. Chem., Int. Ed.*, 2007, **46**, 1318–1320.

10 R. H. Müller and D. L. Clegg, *Anal. Chem.*, 1949, **21**, 1123–1125.

11 A. W. Martinez, S. T. Phillips, Z. Nie, C.-M. Cheng, E. Carrilho, B. J. Wiley and G. M. Whitesides, *Lab Chip*, 2010, **10**, 2499–2504.

12 E. Fu, B. Lutz, P. Kauffman and P. Yager, *Lab Chip*, 2010, **10**, 918–920.

13 G. IJ. Salentijn, H. P. Permentier and E. Verpoorte, *Anal. Chem.*, 2014, **86**, 11657–11665.

14 A. K. Yetisen, M. S. Akram and C. R. Lowe, *Lab Chip*, 2013, **13**, 2210–2251.

15 J. Wang, M. R. N. Monton, X. Zhang, C. D. M. Filipe, R. Pelton and J. D. Brennan, *Lab Chip*, 2014, **14**, 691–695.

16 X. Li, J. Tian and W. Shen, *Cellulose*, 2010, **17**, 649–659.

17 C. A. Schneider, W. S. Rasband and K. W. Eliceiri, *Nat. Methods*, 2012, **9**, 671–675.

18 X. Li, J. Tian, G. Garnier and W. Shen, *Colloids Surf., B*, 2010, **76**, 564–570.

19 S. A. Bhakta, R. Borba, M. Taba Jr., C. D. Garcia and E. Carrilho, *Anal. Chim. Acta*, 2014, **809**, 117–122.

20 E. Washburn, *Phys. Rev.*, 1921, **17**, 273–283.

21 J. Liu, H. Wang, N. E. Manicke, J.-M. Lin, R. G. Cooks and Z. Ouyang, *Anal. Chem.*, 2010, **82**, 2463–2471.

22 D. E. Karcher and M. D. Richardson, *Crop Sci.*, 2003, **43**, 943–951.

23 K. Cantrell, M. M. Erenas, I. De Orbe-Payá and L. F. Capitán-Vallvey, *Anal. Chem.*, 2010, **82**, 531–542.